ACS APPLIED MATERIALS & INTERFACES
Research Article
www.acsami.org

Highly Uniform Resistive Switching Properties of Amorphous InGaZnO Thin Films Prepared by a Low Temperature Photochemical Solution Deposition Method

Wei Hu,[†] Lilan Zou,[†] Xinman Chen,[‡] Ni Qin,[†] Shuwei Li,[†] and Dinghua Bao*,[†]

[†]State Key Laboratory of Optoelectronic Materials and Technologies, School of Physics and Engineering, Sun Yat-Sen University, Guangzhou, Guangdong 510275, China

[‡]Institute of Opto-electronic Materials and Technology, South China Normal University, Guangzhou, Guangdong 510631, China

Supporting Information

ABSTRACT: We report on highly uniform resistive switching properties of amorphous InGaZnO (a-IGZO) thin films. The thin films were fabricated by a low temperature photochemical solution deposition method, a simple process combining chemical solution deposition and ultraviolet (UV) irradiation treatment. The a-IGZO based resistive switching devices exhibit long retention, good endurance, uniform switching voltages, and stable distribution of low and high resistance states. Electrical conduction mechanisms were also discussed on the basis of the current−voltage characteristics and their temperature dependence. The excellent resistive switching properties can be attributed to the reduction of organic- and hydrogen-based elements and the formation of enhanced metal-oxide bonding and metal-hydroxide bonding networks by hydrogen bonding due to UV irradiation, based on Fourier-transform-infrared spectroscopy, X-ray photoelectron spectroscopy, and Field emission scanning electron microscopy analysis of the thin films. This study suggests that a-IGZO thin films have potential applications in resistive random access memory and the low temperature photochemical solution deposition method can find the opportunity for further achieving system on panel applications if the a-IGZO resistive switching cells were integrated with a-IGZO thin film transistors.

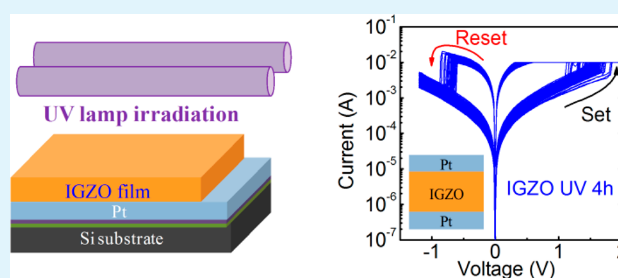

KEYWORDS: *resistive switching, RRAM, InGaZnO, photochemical solution deposition, thin film*

1. INTRODUCTION

Among the emerging memory technologies, resistive switching (RS) effect has attracted significant attention due to the superior performance such as high density and low cost, high endurance and long retention, fast operating speed and low energy consumption for its promising applications in non-volatile resistive random access memory (RRAM), artificial neural computing, and reconfigurable logic operation fields.[1−4] In general, the RS behaviors, exhibiting reproducible switching between high resistance state (HRS) and low resistance state (LRS), have been classified into two types, i.e., the electrical amplitude dependent unipolar RS and the electrical polarity dependent bipolar RS. RS behaviors have been investigated widely in numerous oxide-based materials including binary transition oxides[5−7] and perovskite oxides,[8] as well as spinel oxides.[9,10]

Recently, crystalline ZnO-based thin films were reported to exhibit excellent RS properties.[11,12] Considering that amorphous thin films have high uniformity over a large area, low growth temperature, excellent flexibility, the lack of grain boundaries, and a scalable device to nanometer size and thus benefit high density integration, amorphous ZnO-based thin films have also attracted much attention for possible RRAM applications.[13,14] As a matter of fact, it has been reported that amorphous InGaZnO (a-IGZO) thin films showed remarkable RS properties.[15−19] Note that a-IGZO is also an important electric channel material for use in thin film transistors (TFT) because of its high transparence and high flexibility, high mobility, and low-temperature fabrication process;[20] it should be of great significance to seek a low temperature process to fabricate a-IGZO thin films with high RS performance, and meanwhile, the process can be compatible with the low temperature processed a-IGZO TFT. Thus, it is possible that a-IGZO RS memory cells can be integrated with a-IGZO TFT for achieving system on panel applications. The integration of RS memory cells, with a transistor or a diode, can also effectively solve the so-called sneak path problem caused by parasitic currents through the neighboring memory cells in RRAM devices integrated in passive crossbar arrays.[21]

In this study, a low temperature photochemical solution deposition method combining chemical solution deposition and ultraviolet (UV) irradiation treatment was used to prepare a-IGZO thin films for RRAM applications and for further integrating a-IGZO RS memory cells with a-IGZO TFT to

Received: January 3, 2014
Accepted: March 17, 2014
Published: March 17, 2014

 © 2014 American Chemical Society dx.doi.org/10.1021/am500048y | ACS Appl. Mater. Interfaces 2014, 6, 5012−5017

achieve system on panel applications. We noted that the similar deposition method has been successfully used in the fabrication of a-IGZO TFT devices.[22−24] Kim et al. demonstrated that high performance flexible a-IGZO TFT can be fabricated by a room temperature photochemical activated sol-gel method;[22] Su et al. reported the low temperature solution-processed a-IGZO TFT through ultraviolet-ozone irradiation, and Umeda et al. investigated the impact of UV/O_3 treatment on the performance of solution-processed a-IGZO TFT.[23,24] Therefore, if we could prepare high performance a-IGZO RS cells using the low temperature photochemical solution deposition method, it would be possible to integrate low-temperature processed a-IGZO RS cells with low temperature processed a-IGZO TFT. Our results indicated that, using the low temperature photochemical solution deposition method, a-IGZO thin films can be easily and practically prepared. The thin films sandwiched by Pt electrodes with Pt/a-IGZO/Pt configuration show highly uniform resistive switching behaviors including long retention and good endurance, as well as a stable distribution of high resistance state, low resistance state, and switching voltages.

2. EXPERIMENTAL SECTION

2.1. Fabrication of IGZO Thin Films and Devices. The a-IGZO thin films were prepared by a low temperature photochemical solution deposition method combining chemical solution deposition and UV irradiation treatment. All solvents and chemicals were of reagent quality and were used without further purification. First, the precursor solution of 0.1 M was synthesized using indium(III) nitrate hydrate, gallium(III) nitrate hydrate, and zinc acetate dihydrate as starting materials with an atomic molar ratio of In/Ga/Zn = 1:1:1 and 2-methoxyethanol as solvent. Then, the precursor solution was spun-coated on $Pt/Ti/SiO_2/Si$ substrates at a rotating speed of 3000 rpm for 30 s to obtain wet films. The wet films were baked at 130 °C for 5 min. The above spin-coating and baking procedure was repeated 6 times. Then, the thin films were treated with UV irradiation for 4 h in air at room temperature. Two low-pressure mercury lamps (Philips TUV 8 W, area of 26 × 8 cm^2) were used as the UV light source having a wavelength of 185 nm (10%) and 254 nm (90%). The output energy intensity of the two low-pressure mercury lamps was ∼12.5−13.5 mW/cm^2 measured by FieldMax II (COHERENT) and varied slightly with measurement position. When irradiating the low-pressure mercury lamps in an air atmosphere, ozone is generated due to the combination of O atom and O_2 molecules. Thereafter, the thin films without and with UV irradiation were abbreviated as Non-UV-films and UV-films, respectively. For comparison, the a-IGZO thin films were also prepared under the same deposition conditions and then annealed at 400 °C for 2 h in air without UV irradiation (thereafter, abbreviated as 400°C-films). The circular Pt top electrodes with diameters of 300 μm were deposited on the surface of the a-IGZO thin films using a shadow mask for fabricating the memory devices and investigating the electrical properties.

2.2. Materials Characterizations and Electrical Measurements. The crystalline phase of the thin films was identified using a Rigaku X-ray diffraction (XRD) unit with Cu Kα radiation operated at 40 kV and 25 mA. The cross-sectional morphologies of the thin films were investigated by JSM-6330F field emission scanning electron microscopy (SEM). The Fourier transform-infrared (FT-IR) spectra of the thin films were measured by Nicolet 6700, and the chemical states of the thin films were characterized by X-ray photoelectron spectroscopy (XPS) with ESCALab 250. The XPS spectra of these films were measured after removing the surface contamination by Ar^+ ion sputtering for 30 s at an etching speed of 0.04 nm/s. The current−voltage ($I-V$) characteristics of Pt/a-IGZO/Pt cells were measured at room temperature in air using a Keithley 4200 semiconductor parameter analyzer. During the electrical measurements, the positive bias in voltage sweep mode means that the current flows from the top Pt electrode to the Pt bottom electrode.

3. RESULTS AND DISCUSSION

We investigated the effect of UV irradiation on RS properties of a-IGZO thin films with Pt/a-IGZO/Pt configuration. Before characterizing the RS properties, an electrically forming process is required to trigger the cells from the initial HRS to LRS. Typical $I-V$ behaviors of the electroforming processes of these memory cells and the statistics of the electroforming voltages measured from 10 different memory cells are shown in Figure S1, Supporting Information. After the electroforming process, these memory cells exhibited resistive switching properties. Figure 1a−c shows the $I-V$ characteristics of the three films

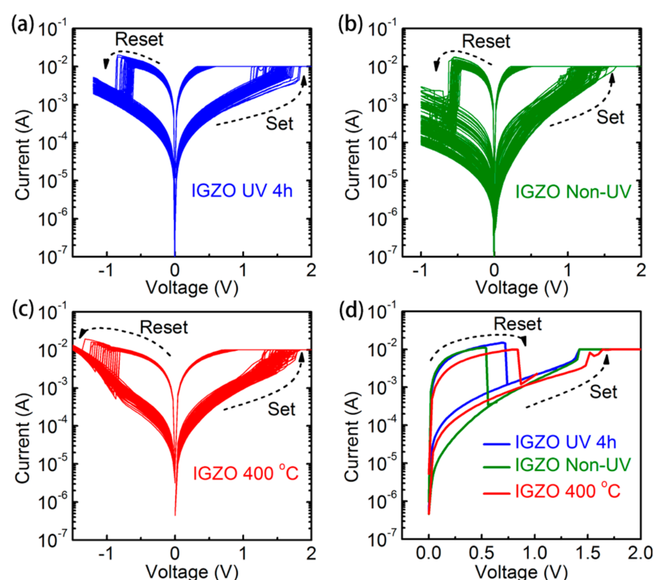

Figure 1. Typical $I-V$ characteristics of (a) UV-films, (b) Non-UV-films, and (c) 400 °C-films. (d) Unipolar $I-V$ behaviors of these memory cells.

(UV-film, Non-UV-film, and 400 °C-film) with Pt top and bottom electrodes, respectively. These cells switched from LRS to HRS as the negative voltage was applied, defined as the reset process, whereas the set process occurred drastically at the positive critical voltage region with a compliance current of 10 mA. In addition, as shown in Figure 1d, the reset and set processes can be carried out in the same voltage polarity regions of these memory cells, demonstrating that the RS properties depend on the voltage magnitude not the polarity of the voltage. Thus, the memory cells exhibit unipolar RS properties.

Figure 2a shows the distribution of the programmed resistance of the three films with Pt top and bottom electrodes obtained by one hundred continuous cycles read at −0.2 V. It is noted that HRS/LRS ratio of these memory cells is larger than 10, which is required to allow for small and highly efficient sense amplifiers to probe the different resistance states. Moreover, the distribution of HRS of the UV-film and the 400 °C-film is more stable and uniform than that of the Non-UV-film. As shown in Figure 2b, the device-to-device statistics of the set and reset switching voltages indicate reasonably controlled and reproducible RS properties in these memory cells. The UV-films exhibit more uniform and concentrated distribution of switching voltages than Non-UV-films and 400

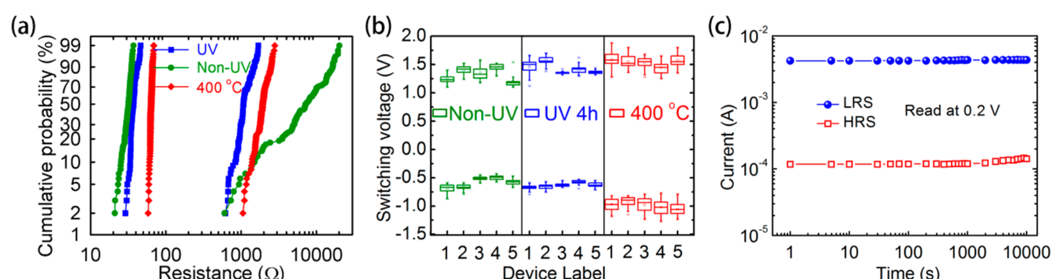

Figure 2. (a) Distribution of the programmed resistance of UV-films, Non-UV-films, and 400 °C-films obtained by one hundred continuous cycles and read at −0.2 V. (b) Set and reset switching voltages distribution of UV-films, Non-UV-films, and 400 °C-films collected from 5 different cells. (c) Retention capability of HRS and LRS in UV-films.

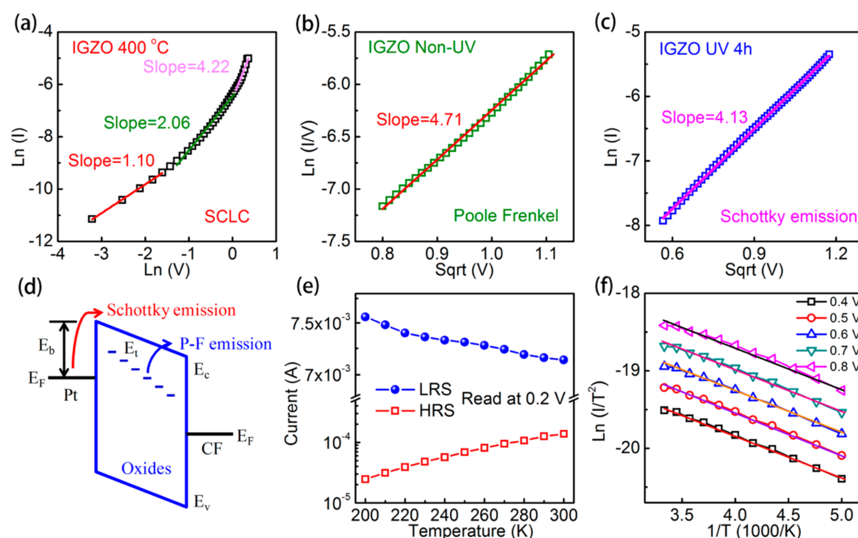

Figure 3. (a) I−V curves plotted by SCLC in HRS of 400 °C-films. (b) I−V curves fitted by Poole-Frenkel emission in HRS of Non-UV-films. (c) I−V curves fitted by Schottky emission in HRS of UV-films. (d) Schematic diagram of electron transport paths of Schottky emission and Poole-Frenkel emission. (e) Temperature dependence of LRS and HRS in UV-films. (f) $\ln(I/T^2)$ versus $1/T$ in HRS of UV-films recorded from 0.4 to 0.8 V.

°C-films. Figure 2c displays the retention capability of HRS and LRS in UV-films, which was obtained under a readout voltage of 0.2 V after switching the devices to HRS or LRS, respectively. The resistance values of both HRS and LRS are stable without degradation over 10^4 s, indicating that the devices are nonvolatile and can be read nondestructively.

Generally, the formation and rupture of the conducting filaments can be accepted to explain the mechanism of unipolar RS. To further understand the conduction mechanism, the I−V curves are fitted to analyze carrier transport in these memory cells. Figure 3a shows the I−V curves of the 400 °C-film plotted by double-ln scale in HRS. The fitting results with solid lines are in good agreement with the trap-controlled space charge limited current (SCLC). In the low voltage region ranging from 0 to ∼0.3 V, the I−V relationship shows a linear dependence on voltage, suggesting an Ohmic conduction region. Following the voltage region, the fitting results indicate that the current obeys the square dependence on voltage, which accords with the Child's square law ($I \sim V^2$). While at the higher voltage region, the current increases fast, correspondingly to the steep increase region in trap-controlled SCLC. It is worth noting that the asymmetric rectifying I−V curves of Non-UV-films are highly reproducible according to Figure 1b. Figure S2, Supporting Information, shows a typical asymmetric I−V curve in HRS of the Non-UV-films in linear scale. To elucidate the asymmetric rectifying behaviors in HRS of the Non-UV-film, we fitted the I−V curves in HRS. At the voltage region from 0.3 to 0.7 V, the I−V curve obeys the linear relation of $\ln(I)$ versus $(V)^{1/2}$, which indicates that the conduction mechanism is dominated by Schottky emission shown in Figure S3, Supporting Information. However, as shown in Figure 3b, in HRS of Non-UV-films, the conduction mechanism is dominated by the Poole-Frenkel emission in the higher voltage region (0.7−1.3 V). This proves that partial defects existed and emitted the electrons in higher voltage in the Non-UV-films according to the schematic diagram of electron transport paths shown in Figure 3d. Furthermore, it is also suggested that the filaments are inclined to rupture in the interface between top Pt electrode and a-IGZO film in terms of the asymmetric rectifying behaviors.[25] The fitted I−V results of the UV-films are shown in Figure 3c. The conduction mechanism in HRS of the UV-films exhibited the symmetric Schottky emission in HRS in spite of the injection of numerous electrons at the high voltage region. The conversion of the conduction mechanism from Poole-Frenkel emission in Non-UV-films to Schottky emission in UV-films indicated theoretically that partial traps were passivated by UV irradiation in the UV-films. Figure 3e shows the temperature dependence of the low and high resistance states of UV-films. The current of LRS decreases with increasing temperature, indicating a metallic conducting behavior. By linearly fitting the

dx.doi.org/10.1021/am500048y | ACS Appl. Mater. Interfaces 2014, 6, 5012−5017

resistance of LRS using the equation $R(T) = R_0[1 + \alpha(T - T_0)]$, the resistance temperature coefficient is determined to be 5.89×10^{-4} K^{-1}. A similar resistance temperature coefficient has been reported for InGaZnO resistive switching devices, and it was suggested that the conducting filaments were mainly composed of oxygen vacancies.[9,17] In contrast, the current value of HRS increases linearly with increasing temperature, which indicates an insulating or semiconducting behavior in HRS. We measured the temperature dependence of the $I-V$ characteristics of HRS in the UV-films as shown in Figure S4, Supporting Information. We attempted to fit the $I-V$ curves using different conduction mechanisms including Schottky emission, Poole-Frenkel model, Fowler-Nordheim model, and SCLC behavior. Our results indicated that the $I-V$ curves can be fitted best with Schottky emission. The Schottky emission can be expressed as:

$$J = A^*T^2\exp[-q(\phi_B - \sqrt{qE/4\pi\varepsilon})/kT] \quad (1)$$

where A^* is the effective Richardson constant, T is the temperature, J is the current density, E is the electric field, ϕ_B is the effective Schottky barrier height, q is the electron charge, ε is the dielectric constant, and k is Boltzmann's constant. The eq 1 can be written as:

$$J/T^2 \propto \exp[q(a\sqrt{V} - \phi_B)/kT] \quad (2)$$

Then,

$$\ln(J/T^2) \propto q(a\sqrt{V} - \phi_B)/kT \quad (3)$$

Thus, for a given voltage, if we draw the plot of $\ln(J/T^2)$ versus $1/T$, a nearly straight line can be obtained. Figure 3f shows the $\ln(I/T^2)$ versus $1/T$ in HRS of UV-films recorded from 0.4 to 0.8 V, the fitted straight lines in the plot of $\ln(I/T^2)$ versus $1/T$ indicated that the conduction mechanism follows Schottky emission.

In order to know why the UV-films have better RS properties than the Non-UV-films and 400 °C-films, we carried out the XRD, FT-IR, SEM, and XPS analyses of the thin films. The three films are amorphous based on the XRD data shown in Figure S5, Supporting Information. Figure 4 shows the FT-IR spectra of the UV-films with different UV irradiation time, the Non-UV-films, and the thin films with an annealing treatment of 350 and 400 °C. The FT-IR spectra of the 350 and 400 °C-films exhibit weak OH stretching bonding and do not show the peaks associated with organic bonding and compounds. However, it can be seen that the broad peak ranging from 2800 to 3700 cm^{-1}, attributed to the OH stretching vibrations, shifts to a low wavenumber gradually as the UV irradiation time increases. It is generally believed that the free state of metal-hydroxide (M-OH) bonding was decomposed and/or transited to the state of M-OH bonding network with hydrogen bonding.[24] The sharp peaks at 1590, 1420, and 1350 cm^{-1} are assigned to the C−O and C−C stretching vibrations for the Non-UV-films. These sharp peaks disappear, and two new symmetric broad peaks are observed in the thin films with UV irradiation above 4 h, indicating that C−O and C−C bonding were decomposed and graphite-like carbon or disordered carbon formed probably.[24,27]

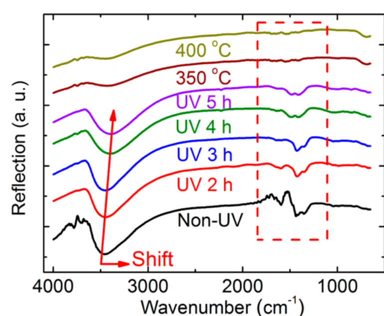

Figure 4. FT-IR spectra of a-IGZO thin films with different treatments.

Figure 5a shows the cross-sectional SEM images of these three films. As can be seen, the thickness of the 400 °C-films is thinner than that of UV-films and Non-UV-films, and the thickness of UV-films is thinner than that of Non-UV-films, implying that organic- and hydrogen-based elements were reduced through thermal-annealing or UV treatment. Figure 5b shows the XPS narrow-scan spectra of O1s for the Non-UV-films, UV-films, and the 400 °C-films in the same scale. The O1s spectrum of the Non-UV-films and UV-films can be resolved into three peaks at 530.58, 532.02, and 533.10 eV, which correspond to the metal-oxide (M-O) bonding, M-OH bonding, and related C−O bonding, respectively. Compared to the Non-UV-films, the intensity of the M-O bonding and M-OH bonding in UV-films were enhanced. However, the O1s spectrum of the 400 °C-films can be only fitted by two peaks centered at 530.62 and 531.90 eV, which can be assigned to M-O bonding and defective oxygen state. No fitted peak assigned to the M-OH bonding can be seen, implying that all the residual organic- and hydrogen-based elements have been removed by annealing treatment. Meanwhile, In 3d, Ga 2p, and Zn 2p core-level XPS spectra of the Non-UV-films, UV-films, and 400 °C-films, corresponding to In−O bonding, Ga−O bonding, and Zn−O bonding, are shown in Figures S6, S7, and S8, Supporting Information, respectively. Especially, the intensity of In 3d and Ga 2p peaks of UV-films and 400 °C-films were enhanced obviously in comparison with Non-UV-films. This is also consistent with the O 1s XPS result. Therefore, on the basis of the above analysis, the formation and rupture of filaments could be controlled and stabilized in local domains as a result of the reduction of organic- and hydrogen-based elements and the formation of enhanced M-O bonding and M-OH bonding networks by hydrogen bonding or the passivation of charge traps by hydrogen bonding in the UV-films, which might be responsible for the excellent RS

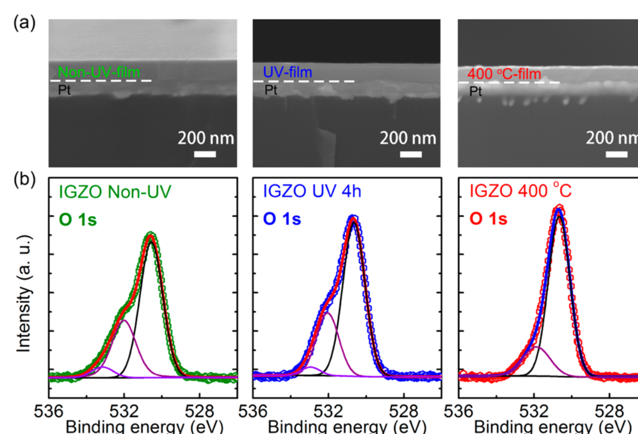

Figure 5. (a) Cross-sectional SEM images of a-IGZO Non-UV-films, UV-films, and 400 °C-films. (b) O 1s XPS spectra of a-IGZO Non-UV-films, UV-films, and 400 °C-films.

dx.doi.org/10.1021/am500048y | ACS Appl. Mater. Interfaces 2014, 6, 5012−5017

performance such as uniform switching voltages and stable distribution of HRS and LRS. The passivation of charge traps by hydrogen bonding for high performance a-IGZO TFT has also been reported.[26,28]

4. CONCLUSIONS

In conclusion, the a-IGZO thin films have been fabricated by a low temperature photochemical solution deposition method combining chemical solution deposition and ultraviolet irradiation treatment. The Pt/a-IGZO/Pt cells show reproducible and highly uniform RS properties in set and reset switching voltages as well as the stable distribution of LRS and HRS. The high uniformity of the RS properties can be attributed to reduction of residual content and formation of enhanced M-O bonding and M-OH bonding by hydrogen bonding as well as passivation of charge traps by hydrogen bonding. Our results also suggest that the low temperature photochemical solution deposition method can find the opportunity for achieving system on panel applications if the RS cells were integrated with the low temperature processed a-IGZO TFT.

■ ASSOCIATED CONTENT

Supporting Information

Typical *I*−*V* behaviors of the electroforming processes; statistics of the electroforming voltages; asymmetric *I*−*V* curves in HRS of the Non-UV-films; *I*−*V* curves fitted by Schottky emission in HRS of Non-UV-films; *I*−*V* curves of HRS of UV-films depending on temperature; XRD patterns of IGZO UV-films, Non-UV-films, and 400 °C-films; In 3d, Ga 2p, and Zn 2p core-level XPS spectra of Non-UV-films, UV-films, and 400 °C-films. This information is available free of charge via the Internet at http://pubs.acs.org.

■ AUTHOR INFORMATION

Corresponding Author

*E-mail: stsbdh@mail.sysu.edu.cn.

Notes

The authors declare no competing financial interest.

■ ACKNOWLEDGMENTS

The authors gratefully acknowledge financial support from Natural Science Foundation of China (Nos. 51372281 and 61204102), National Basic Research Program (973 Program) of China (No. 2012CB619302), and the Scholarship Award for Excellent Doctoral Student granted by Ministry of Education of China (No. 300003191007).

■ REFERENCES

(1) Waser, R.; Aono, M. Nanoionics-Based Resistive Switching Memories. *Nat. Mater.* **2007**, *6*, 833−840.

(2) Waser, R.; Dittmann, R.; Staikov, G.; Szot, K. Redox-Based Resistive Switching Memories-Nanoionic Mechanisms, Prospects, and Challenges. *Adv. Mater.* **2009**, *21*, 2632−2663.

(3) Yang, J. J.; Strukov, D. B.; Strewart, D. R. Memristive Devices for Computing. *Nat. Nanotechnol.* **2013**, *8*, 13−24.

(4) Wong, H.-S. P.; Lee, H. Y.; Yu, S. M.; Chen, Y. S.; Wu, Y.; Chen, P. S.; Lee, B.; Chen, F. T.; Tsai, M. J. Metal-Oxide RRAM. *Proc. IEEE* **2012**, *100*, 1951−1970.

(5) Strukov, D. B.; Sinder, G. S.; Stewart, D. R.; Williams, R. S. The Missing Memristor Found. *Nature* **2008**, *453*, 80−83.

(6) Yu, S. M.; Chen, H. Y.; Gao, B.; Kang, J. F.; Wong, H.-S. P. HfO_x-Based Vertical Resistive Switching Random Access Memory Suitable for Bit-Cost-Effective Three-Dimensional Cross-Point Architecture. *ACS Nano* **2013**, *7*, 2320−2325.

(7) Lee, M. J.; Lee, C. B.; Lee, D.; Lee, S. R.; Chang, M.; Hur, J. H.; Kim, Y. B.; Kim, C. J.; Seo, D. H.; Seo, S.; Chung, U. I.; Yoo, I. K.; Kim, K. A Fast, High-Endurance and Scalable Non-Volatile Memory Device Made from Asymmetric Ta_2O_{5-x}/TaO_{2-x} Bilayer Structures. *Nat. Mater.* **2011**, *10*, 625−630.

(8) Chen, X.; Wu, N. J.; Strozier, J.; Ignatiev, A. Spatially Extended Nature of Resistive Switching in Perovskite Oxide Thin Films. *Appl. Phys. Lett.* **2006**, *89*, 063507.

(9) Hu, W.; Qin, N.; Wu, G. H.; Lin, Y. T.; Li, S. W.; Bao, D. H. Opportunity of Spinel Ferrite Materials in Nonvolatile Memory Device Applications Based on Their Resistive Switching Performances. *J. Am. Chem. Soc.* **2012**, *134*, 14658−14661.

(10) Hu, W.; Chen, X. M.; Wu, G. H.; Lin, Y. T.; Qin, N.; Bao, D. H. Bipolar and Tri-State Unipolar Resistive Switching Behaviors in Ag/$ZnFe_2O_4$/Pt Memory Devices. *Appl. Phys. Lett.* **2012**, *101*, 063501.

(11) Chen, X. M.; Wu, G. H.; Jiang, P.; Liu, W. F.; Bao, D. H. Colossal Resistance Switching Effect in Pt/spinel-MgZnO/Pt Devices for Nonvolatile Memory Applications. *Appl. Phys. Lett.* **2009**, *94*, 033501.

(12) Chen, X. M.; Wu, G. H.; Bao, D. H. Resistive Switching Behavior of Pt/$Mg_{0.2}Zn_{0.8}O$/Pt Devices for Nonvolatile Memory Applications. *Appl. Phys. Lett.* **2008**, *93*, 093501.

(13) Huang, C. H.; Huang, J. S.; Lai, C. C.; Huang, H. W.; Lin, S. J.; Chueh, Y. L. Manipulated Transformation of Filamentary and Homogeneous Resistive Switching on ZnO Thin Film Memristor with Controllable Multistate. *ACS Appl. Mater. Interfaces* **2013**, *5*, 6017−6023.

(14) Chen, J. Y.; Hsin, C. L.; Huang, C. W.; Chiu, C. H.; Huang, Y. T.; Lin, S. J.; Wu, W. W.; Chen, L. J. Dynamic Evolution of Conducting Nanofilament in Resistive Switching Memories. *Nano Lett.* **2013**, *13*, 3671−3677.

(15) Chen, M. C.; Chang, T. C.; Tsai, C. T.; Huang, S. Y.; Chen, S. C.; Hu, C. W.; Sze, S. M.; Tsai, M. J. Influence of Electrode Material on The Resistive Memory Switching Property of Indium Gallium Zinc Oxide Thin Films. *Appl. Phys. Lett.* **2010**, *96*, 262110.

(16) Kim, C. H.; Jang, Y. H.; Hwang, H. J.; Song, C. H.; Yang, Y. S.; Cho, J. H. Bistable Resistance Memory Switching Effect in Amorphous InGaZnO Thin Films. *Appl. Phys. Lett.* **2010**, *97*, 062109.

(17) Wang, Z. Q.; Xu, H. Y.; Li, X. H.; Zhang, X. T.; Liu, Y. X.; Liu, Y. C. Flexible Resistive Switching Memory Device Based on Amorphous InGaZnO Film with Excellent Mechanical Endurance. *IEEE Electron Device Lett.* **2011**, *32*, 1442−1444.

(18) Hsu, C. H.; Fan, Y. S.; Liu, P. T. Multilevel Resistive Switching Memory with Amorphous InGaZnO-Based Thin Film. *Appl. Phys. Lett.* **2013**, *102*, 062905.

(19) Wang, Z. Q.; Xu, H. Y.; Li, X. H.; Yu, H.; Liu, Y. C.; Zhu, X. J. Synaptic Learning and Memory Functions Achieved Using Oxygen Ion Migration/Diffusion in an Amorphous InGaZnO Memristor. *Adv. Funct. Mater.* **2012**, *22*, 2759−2765.

(20) Nomura, K.; Ohta, H.; Takagi, A.; Kamiya, T.; Hirano, M.; Hosono, H. Room-Temperature Fabrication of Transparent Flexible Thin-Film Transistors Using Amorphous Oxide Semiconductors. *Nature* **2004**, *432*, 488−492.

(21) Linn, E.; Rosezin, R.; Kugeler, C.; Waser, R. Complementary Resistive Switches for Passive Nanocrossbar Memories. *Nat. Mater.* **2010**, *9*, 403−406.

(22) Kim, Y. H.; Heo, J. S.; Kim, T. H.; Park, S.; Yoon, M. H.; Kim, J.; Oh, M. S.; Yi, G. R.; Noh, Y. Y.; Park, S. K. Flexible Metal-Oxide Devices Made by Room-Temperature Photochemical Activation of Sol-Gel Films. *Nature* **2012**, *489*, 128−132.

(23) Su, B. Y.; Chu, S. Y.; Juang, Y. D.; Chen, H. C. High-Performance Low-Temperature Solution-Processed InGaZnO Thin-Film Transistors via Ultraviolet-Ozone Photo-Annealing. *Appl. Phys. Lett.* **2013**, *102*, 192101.

(24) Umeda, K.; Miyasako, T.; Sugiyama, A.; Tanaka, A.; Suzuki, M.; Tokumitsu, E.; Shimoda, T. Impact of UV/O_3 Treatment on Solution-

Processed Amorphous $InGaZnO_4$ Thin-Film Transistors. *J. Appl. Phys.* **2013**, *113*, 184509.
(25) Nam, Y.; Hwang, I.; Oh, S.; Lee, S.; Lee, K.; Hong, S.; Kim, J.; Choi, T.; Park, B. H. Switchable Schottky Diode Characteristics Induced by Electroforming Process in Mn-Doped ZnO Thin Films. *Appl. Phys. Lett.* **2013**, *102*, 162105.
(26) Tsao, S. W.; Chang, T. C.; Huang, S. Y.; Chen, M. C.; Chen, S. C.; Tsai, C. T.; Kuo, Y. J.; Chen, Y. C.; Wu, W. C. Hydrogen-Induced Improvements in Electrical Characteristics of a-IGZO Thin-Film Transistors. *Solid-State Electron.* **2010**, *54*, 1497−1499.
(27) Ferrari, A. C.; Robertson, J. Interpretation of Raman Spectra of Disordered and Amorphous Carbon. *Phys. Rev. B* **2000**, *61*, 14095−14107.
(28) Oh, S.-I.; Choi, G.; Hwang, H.; Lu, W.; Jang, J.-H. Hydrogenated IGZO Thin-Film Transistors Using High-Pressure Hydrogen Annealing. *IEEE Trans. Electron Devices* **2013**, *60*, 2537−2541.